PHYSICAL REVIEW B **89**, 201414(R) (2014)

All-optical approach to determine the spatial shape of nanoscale electron wave functions using intraband spectroscopy

Sandra C. Kuhn, Andreas Knorr, and Marten Richter
Institut für Theoretische Physik, Nichtlineare Optik und Quantenelektronik, Technische Universität Berlin, Hardenbergstrasse 36, EW 7-1, 10623 Berlin, Germany

Nina Owschimikow, Mirco Kolarczik, Yücel I. Kaptan, and Ulrike Woggon
Institut für Optik und Atomare Physik, Technische Universität Berlin, Straße des 17. Juni, ER 1-1, 10623 Berlin, Germany
(Received 10 October 2013; published 29 May 2014)

A spectroscopic pump-probe method to determine the spatial shape of bound quantum states in semiconductor quantum dots is proposed. The method uses intraband transitions between the bound states and unbound continuum states in the host medium. The developed theoretical scheme is applicable to quantum dots embedded in bulk material and with some modification also for other nanostructures. In particular, the analyzed pump-probe spectra exhibit specific spectral signatures for different spatial extensions of the quantum dot confinement potential.

DOI: 10.1103/PhysRevB.89.201414 PACS number(s): 78.67.Hc, 73.21.La, 73.22.Dj, 78.47.−p

Due to their unique optical and transport properties, semiconductor quantum dots (QDs) are one of the most extensively studied nanostructures. They are used in a variety of applications such as QD lasers [1], light-emitting diodes [2], single photon emitters [3,4], and solar cells [5]. These applications are made possible by an improvement of crystal growth, e.g., molecular beam epitaxy (MBE) [6] and metal-organic chemical-vapor deposition (MOCVD) [7]. For example, self-organized InAs/GaAs QDs can be fabricated by Stranski-Krastanow [8,9] and Volmer-Weber [8] growth, which results in different sizes and shapes of the QDs. However, high quality devices, for instance, sources for nonclassical light [10], require precise information about the structural properties of the QDs [11].

In this respect, electron microscope techniques or scanning tunneling microscopes are used to obtain information on the growth, the self-assembling, and the structural properties, especially the QD shape and size [12–14]. However, they do not offer direct access to the shape of the electron (hole) wave function. In Refs. [15–18] interband photoluminescence spectroscopy is used to retrieve a parametrized exciton wave function. There, a specific model for the QD potential is assumed and thus the shape of the wave function is already implicitly assumed but not directly determined. The dispersion of the QD size can be estimated [19,20], but it does not provide the spatial shape of the wave function.

In this Rapid Communication, we propose an all-optical approach, which has a direct access to the spatial shape of the ground state wave function. In particular, the electron and hole wave function can be extracted separately. Our method exploits optical transitions between the bound QD (localized inside the QD) and unbound continuum states (located in the surrounding host medium). The investigation of bound-continuum transitions is similar to angle-resolved photoemission spectroscopy measurements [21] in which the transitions between bound and continuum states are used to observe the distribution of the electrons in the reciprocal space. We derive a relation between the Fourier transform of the QD ground state wave function and the optical intraband spectra, unraveling spatial information encoded in the optical spectra.

Corresponding experimental realizations come in different forms, e.g., pulsed pump-probe experiments [22–25] or continuous wave spectroscopy. Also single beam experiments for doped QDs are possible: The only important prerequisites are an occupied bound conduction (valence) band ground state and the ability to optically probe bound to continuum transitions. Here we use pump-probe experiments. All results, however, are obtained in the frequency domain and apply equally to continuous wave excitation.

To illustrate the proposed all-optical scheme to determine a QD wave function, we use an epitaxially grown InAs QD embedded in GaAs bulk material (e.g., Volmer-Weber growth mode) as the model system [8]. However, a much more general statement can be made: The developed method is applicable to determine ground state wave functions if optical transitions of this wave function to a continuum of free carriers can be excited. The all-optical method is similar to angle-resolved photoemission spectroscopy measurements of atomic systems [21]: Besides QDs, other structures of different materials can be described with modifications by our theoretical results. This includes impurities in bulk or other lower dimensional structures such as quantum wells and wires [26]. Also QDs in quantum wires [27] or QD molecule systems [28], for example, QD superstructures [29], may be investigated.

To start, we briefly summarize the possible QD optical transitions in Fig. 1(a). There are interband transitions between bound valence (v) and conduction (c) band states i and j as well as intraband transitions between continuous bulk states $\mathbf{k}$ and bound QD states. For both bands, bound states localized at the QD and unbound bulk continuum states exist. The continuum states are characterized by a wave vector $\mathbf{k}$.

The energy difference between the bound QD state with the lowest (highest) energy and the lowest (highest) bulk state in the conduction (valence) band ΔE_c^i (ΔE_v^j) determines the spectral range of interest [cf. Fig. 1(a)]. Note that the depicted energy gap $\Delta E_{c,v}^i$ depends on the spatial extension of the QD potential.

The proposed experimental scheme to determine the spatial shape of the wave function in the QD is a nonlinear two-step

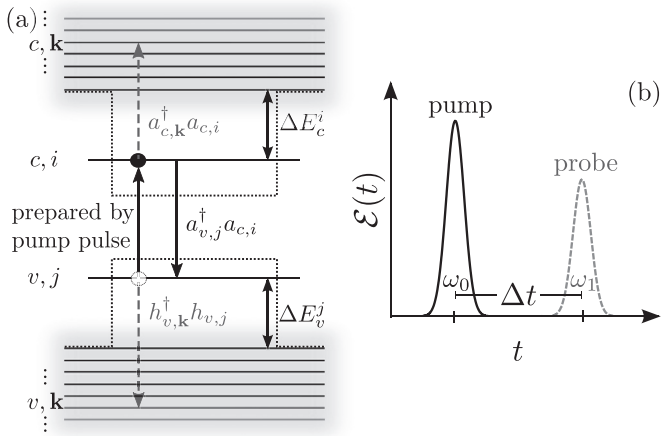

FIG. 1. (a) Level scheme of the QD model: The bulk states have a crystal momentum $\mathbf{k}$. i and j represent the QD levels. The energy difference between the QD state i (j) and the lowest (highest) energy bulk state in the conduction (valence) band is ΔE^i_c (ΔE^j_v). Three transitions are depicted: the interband transition inside the QD, described by $a^\dagger_{v,j}a_{c,i}$, and the transitions between the dot levels and the bulk states $a^\dagger_{c,\mathbf{k}}a_{c,i}$ and $h^\dagger_{v,\mathbf{k}}h_{v,j}$. (b) Pump and probe pulse exciting the QD.

process [cf. Fig. 1(b)]: First, a pump pulse resonantly excites the confined interband electron-hole transition [solid line in Fig. 1(a)]. The pump pulse creates low, but finite, electron and hole populations in the confined QD states. In a second step, a probe pulse tests the intraband transitions resulting from the pump created electron and hole populations [cf. dashed lines in Fig. 1(a)]. We assume that the pump pulse induced coherence is already dephased, when the probe pulse arrives. We show that the spectrally resolved intraband probe absorption contains information about the spatial shape of the QD ground state wave function.

The Hamiltonian H consists of the free electronic contributions H_0, and H_L, which contains the interaction of electrons and the classical light field,

$$H_0 = \sum_{i,\lambda} \epsilon_{\lambda,i} a^\dagger_{\lambda,i} a_{\lambda,i} + \sum_{\mathbf{k},\lambda} \epsilon_{\lambda,\mathbf{k}} a^\dagger_{\lambda,\mathbf{k}} a_{\lambda,\mathbf{k}}, \tag{1}$$

where $\epsilon_{\lambda,i(\mathbf{k})}$ is the energy with the band index $\lambda \in \{c,v\}$ and $a^\dagger_{\lambda,i(\mathbf{k})}$ ($a_{\lambda,i(\mathbf{k})}$) are the creation (annihilation) operators for electrons of the ith bound QD state or the continuum state with wave vector $\mathbf{k}$, respectively.

In the dipole approximation the interaction of the electrons with the external light field $\mathbf{E}(t) = \mathcal{E}(t)\mathbf{e}_\xi$ (polarization direction $\mathbf{e}_\xi$) reads

$$H_\mathrm{L} = -\sum_{i,j} d^{cv}_{ij} \mathcal{E}(t) a^\dagger_{c,i} a_{v,j} - \sum_{i,\mathbf{k},\lambda} d^{\lambda\lambda}_{i\mathbf{k}} \mathcal{E}(t) a^\dagger_{\lambda,i} a_{\lambda,\mathbf{k}} + \mathrm{H.a.} \tag{2}$$

We include QD interband transitions (first contribution) and QD-bulk intraband transitions (second contribution) in Eq. (2). d^{cv}_{ij} and $d^{\lambda\lambda}_{i\mathbf{k}}$ ($\lambda \in \{c,v\}$) are the interband and intraband dipole matrix elements, respectively, in the $\mathbf{e}_\xi$ direction.

Interband transitions start at higher energies and are separated from the intraband spectrum. We assume a radial symmetric system, therefore it is sufficient to reduce the calculation of the absorption to one direction $\mathbf{e}_\xi$. However, measurements of varying probe polarization directions could also give information about the azimuthal symmetry of the QD, because the polarization direction enters on the right-hand side of Eq. (11). A broken azimuthal symmetry should be visible in a polarization diagram of the absorption. The spectral absorption of the probe pulse $\mathcal{E}(\omega)$ can be calculated via the macroscopic polarization $\mathbf{P}_\mathrm{intra}(\omega) = \mathcal{P}_\mathrm{intra}(\omega)\mathbf{e}_\xi$ [30],

$$\alpha(\omega) = \frac{\omega}{nc\epsilon_0} \mathrm{Im}\left[\frac{\mathcal{P}_\mathrm{intra}(\omega)}{\mathcal{E}(\omega)}\right]. \tag{3}$$

Here n is the constant background refractive index around the relevant transition frequencies. The probe pulse $\mathcal{E}(t)$ induces the probe polarization $\mathcal{P}_\mathrm{intra}(t)$,

$$\mathcal{P}_\mathrm{intra}(t) = \rho_\mathrm{QD} \sum_{i,\mathbf{k},\lambda} d^{\lambda\lambda}_{i\mathbf{k}} \langle a^\dagger_{\lambda,i} a_{\lambda,\mathbf{k}} \rangle(t) + \mathrm{c.c.}, \tag{4}$$

where ρ_QD denotes the QD volume density. Using the Heisenberg equation of motion, we calculate the transition amplitudes $p^{\lambda\lambda}_{i\mathbf{k}} = \langle a^\dagger_{\lambda,i} a_{\lambda,\mathbf{k}} \rangle$,

$$\begin{aligned} \partial_t p^{\lambda\lambda}_{i\mathbf{k}}(t) = {} & \frac{i}{\hbar}(\epsilon_{\lambda,i} - \epsilon_{\lambda,\mathbf{k}} + i\gamma) p^{\lambda\lambda}_{i\mathbf{k}}(t) \\ & + \frac{i}{\hbar} d^{\lambda\lambda}_{\mathbf{k}i} \mathcal{E}(t)(f^{\lambda,i} - f^{\lambda,\mathbf{k}}), \end{aligned} \tag{5}$$

introducing a phenomenological dephasing γ. Equation (5) can be solved in Fourier space assuming constant carrier densities $f^{\lambda,i(\mathbf{k})} = \langle a^\dagger_{\lambda,i(\mathbf{k})} a_{\lambda,i(\mathbf{k})} \rangle$ of band λ and state $i(\mathbf{k})$,

$$p^{\lambda\lambda}_{i\mathbf{k}}(\omega) = -\frac{d^{\lambda\lambda}_{\mathbf{k}i} \mathcal{E}(\omega)}{(\epsilon_{\lambda,i} - \epsilon_{\lambda,\mathbf{k}} + \hbar\omega + i\gamma)}(f^{\lambda,i} - f^{\lambda,\mathbf{k}}). \tag{6}$$

Without electrically injected carriers there is no electron (hole) distribution in the bulk conduction (valence) band: $f^{c,\mathbf{k}} = 0$ and $f^{v,\mathbf{k}} = 1$. Using Eq. (6) in Eq. (4) we separate the intraband transitions induced by the probe pulse into the QD-electron-bulk and QD-hole-bulk transitions,

$$\mathcal{P}_\mathrm{intra}(\omega) = \rho_\mathrm{QD} \left(\sum_i \mathcal{P}^c_i(\omega) f^{e,i} + \sum_j \mathcal{P}^v_j(\omega) f^{h,j} \right), \tag{7}$$

where

$$\mathcal{P}^\lambda_i(\omega) \equiv -\sum_{\mathbf{k}} \frac{\left| d^{\lambda\lambda}_{i\mathbf{k}} \right|^2 \mathcal{E}(\omega)}{\left(\Delta\epsilon^\lambda_{i\mathbf{k}} + \hbar\omega + i\gamma \right)}, \tag{8}$$

with the QD-bulk energy differences $\Delta\epsilon^c_{i\mathbf{k}} \equiv \epsilon_{c,i} - \epsilon_{c,\mathbf{k}}$ and $\Delta\epsilon^v_{i\mathbf{k}} \equiv \epsilon_{v,\mathbf{k}} - \epsilon_{v,i}$. $f^{e,i} = \langle a^\dagger_{c,i} a_{c,i} \rangle$ and $f^{h,j} = 1 - \langle a^\dagger_{v,j} a_{v,j} \rangle$ denote the pump induced electron and hole occupations. Equations (7) and (8) show that the contributions from hole and electron intraband transitions occur independently and do not depend on the other carrier system. This is in strong contrast to interband transitions in the QD depending on the sum of the hole $f^{h,j}$ and electron density $f^{e,i}$. Therefore, the absorption spectrum is split up into an electron and a hole contribution,

$$\alpha^i_\lambda(\omega) \equiv \frac{\omega}{nc\epsilon_0} \mathrm{Im}\left[\frac{\mathcal{P}^\lambda_i(\omega)}{\mathcal{E}(\omega)}\right]. \tag{9}$$

All of the following relations hold for electron and hole transitions ($\lambda \in \{c,v\}$), respectively. The contributions are calculated independently and added at the end. Depending on the carrier system (electron, hole), Eq. (9) results in contributions at different energies. Since the spectral contribution of the electronic conduction band transitions is well separated from the hole continuum band transitions and the transitions between the bound states are relatively sharp, we can assume that the electronic contribution $\alpha_c^i(\omega)$ is directly available from experiments. Therefore, results are shown only for the electron contribution to demonstrate the procedure. We have also checked the qualitative behavior for the hole wave functions with similar results. To illustrate the basic principle, we restrict our analysis to intraband transitions from the QD (bound) ground state ($i = 0$).

Now we provide more analytical insight to illustrate that the spatial information can be obtained from Eqs. (7)–(9). For QD intraband transitions, typically the dephasing γ is on the order of few meV [31], which is very small compared to the transition energies (order of eV). Therefore, we assume $\gamma \to 0$ to obtain the absorption

$$\alpha_\lambda^i(\omega) = \frac{V_b \omega}{8\pi^2 nc\epsilon_0} \int d\mathbf{k} \left| d_{i\mathbf{k}}^{\lambda\lambda} \right|^2 \delta\left(\Delta\epsilon_{ik}^\lambda + \hbar\omega\right), \tag{10}$$

with the Dirac delta function $\delta(\Delta\epsilon_{ik}^\lambda + \hbar\omega)$ and the bulk volume V_b. $\alpha_\lambda^i(\omega)$ in Eq. (10) is determined by the squared dipole moment $|d_{i\mathbf{k}}^{\lambda\lambda}|^2$ and the density of states. Calculating the integral, Eq. (10), the density of states at $\Delta\epsilon_{ik}^\lambda + \hbar\omega$ enters. For a first insight, plane waves $\phi_{\lambda,\mathbf{k}}(\mathbf{r}) = \frac{1}{\sqrt{V_b}} e^{i\mathbf{k}\cdot\mathbf{r}}$ are used for the continuum wave functions (improved calculations are given below). Then the intraband dipole moment reads

$$d_{i\mathbf{k}}^{\lambda\lambda} = \frac{q}{\sqrt{V_b}} \int \phi_{\lambda,i}^*(\mathbf{r}) r_\xi e^{i\mathbf{k}\cdot\mathbf{r}} d\mathbf{r} = -\frac{iq}{\sqrt{V_b}} \frac{\partial}{\partial_{k_\xi}} \widetilde{\phi}_{\lambda,i}^*(\mathbf{k}). \tag{11}$$

Here, $\phi_{\lambda,i}^*(\mathbf{r})$ [$\widetilde{\phi}_{\lambda,i}^*(\mathbf{k})$] is the QD ground state wave function in real [Fourier] space, $r_\xi = \mathbf{e}_\xi \cdot \mathbf{r}$, $\frac{\partial}{\partial_{k_\xi}} = \mathbf{e}_\xi \cdot \boldsymbol{\nabla}_\mathbf{k}$, and q is the electron charge. Obviously, for the plane wave approximation, the dipole moment $d_{i\mathbf{k}}^{\lambda\lambda}$ is directly connected to the derivative of the QD ground state wave function $\widetilde{\phi}_{\lambda,i}^*(\mathbf{k})$ in the $\mathbf{k}$ domain. Therefore, the dipole moment $d_{i\mathbf{k}}^{\lambda\lambda}$ in $\alpha_\lambda^i(\omega)$ [Eq. (10)] provides information about the spatial shape of the QD ground state wave function, which can be extracted from the intraband absorption spectrum Eq. (10).

If the band structure of the QD surrounding the bulk material is assumed to be parabolic [32],

$$\epsilon_{c,k} = \frac{\hbar^2 k^2}{2m_e} + \Delta E_c^0 + \epsilon_{c,0}, \tag{12}$$

we can calculate the spectrum $\alpha_\lambda^i(\omega)$ using Eqs. (10)–(12),

$$\alpha_\lambda^i(\omega) = B\omega\sqrt{\hbar\omega - \Delta E_\lambda^i} \left| \frac{\partial}{\partial k} \widetilde{\phi}_{\lambda,i}(k)|_{k=k_0} \right|^2 \Theta\left(\hbar\omega - \Delta E_\lambda^i\right), \tag{13}$$

where $B = \frac{q^2 m^{\frac{3}{2}}}{3\sqrt{2}\pi\hbar^3 nc\epsilon_0}$, $k_0(\omega) = \sqrt{\frac{2m(\hbar\omega - \Delta E_\lambda^i)}{\hbar^2}}$, and $\Theta(\hbar\omega - \Delta E_\lambda^i)$ is the Heaviside function. The intraband absorption is determined by a typical square root dependence on the energy detuning with respect to the gap ΔE_λ^i and the gradient of $\widetilde{\phi}_{\lambda,i}(k)$ at $k_0(\omega)$. We define $\tilde{\alpha}_\lambda^i(\omega) = \frac{\alpha_\lambda^i(\omega)}{\omega}$,

$$\tilde{\alpha}_\lambda^i(k_0) = B\frac{k_0\hbar}{\sqrt{2m}} \left| \frac{\partial}{\partial k_0} \widetilde{\phi}_{\lambda,i}(k_0) \right|^2, \tag{14}$$

and find for these $\widetilde{\phi}_{\lambda,i}(\mathbf{k})$,

$$\left(\frac{\tilde{\alpha}_\lambda^i(k_0)\sqrt{2m}}{Bk_0\hbar} \right)^{\frac{1}{2}} = \left| \frac{\partial}{\partial k_0} \widetilde{\phi}_{\lambda,i}(k_0) \right|. \tag{15}$$

Assuming a monotonic behavior of the QD wave function in the k domain (typically valid for QD ground states $i = 0$), one can write

$$\frac{(2m)^{\frac{1}{4}}}{\sqrt{B\hbar}} \int_0^{k_0} \left(\frac{\tilde{\alpha}_\lambda^0(k_0')}{k_0'} \right)^{\frac{1}{2}} dk_0' = \pm[\widetilde{\phi}_{\lambda,0}(k_0) - \widetilde{\phi}_{\lambda,0}(0)]. \tag{16}$$

Equation (16) and its use to obtain the QD wave function constitutes the main result of this work. It offers the possibility to reconstruct the QD ground state wave function $\phi_{\lambda,0}$ from a measured intraband spectrum: Measuring $\tilde{\alpha}_\lambda^0(\omega)$ [or $\alpha_\lambda^0(\omega)$, respectively] and calculating the left-hand side of Eq. (16) provides the Fourier transform of the QD ground state wave function $\widetilde{\phi}_{\lambda,0}(k_0)$. The width of $\widetilde{\phi}_{\lambda,0}(k_0)$ gives direct access to the spatial QD shape.

However, one important point needs to be checked: The plane wave approximation used so far neglects the dependence of the bulk continuum wave functions on the QD confinement potential. Since Eq. (13) is derived using plane waves, the validity of Eq. (16) for the correct unbound states of a QD continuum system needs to be investigated. We numerically studied several confinement potentials such as rectangular potential wells, and hyperbolic secant-shaped or harmonic potentials. We find that our calculation based on Eq. (16) does not strongly depend on the potential shape. Here, we only give results for the inverse hyperbolic secant potential [cf. Fig. 2(a)],

$$V_a(r) = -\frac{V_0}{\cosh^2\left(\frac{r}{a}\right)}, \tag{17}$$

with height V_0 [33,34] and extension a. As can be see by Eq. (16), the method does not require knowledge of the potential.

To determine the intraband absorption, the wave functions for $V_a(r)$ [35] are calculated numerically using a finite element method (FEM) solver [36]. We assume spherical QDs with typical parameters such as $\Delta E_c^0 \approx 200$ meV for the conduction intraband transition [37] and the effective mass of GaAs [38]. We use the ansatz $\phi(\mathbf{r}) = Y_l^m(\theta,\phi)R_l(r)$ for the envelope part of the wave function and solve the radial Schrödinger equation for $R_0(r)$. The resulting QD bound ground state wave functions are depicted in Fig. 2(b) for different extensions of the QD potential a. To directly compare with literature [39,40], we describe the spatial extension of the QD potential by the localization lengths r^0 [given by the full width at half maximum (FWHM) of the QD bound ground state wave functions]. Typical values of the localization length r^0 of self-assembled QDs are between $r^0 = 3$ and 6 nm [39,40]. The unbound continuum bulk wave functions, resulting from the numerical calculations, have discrete en-

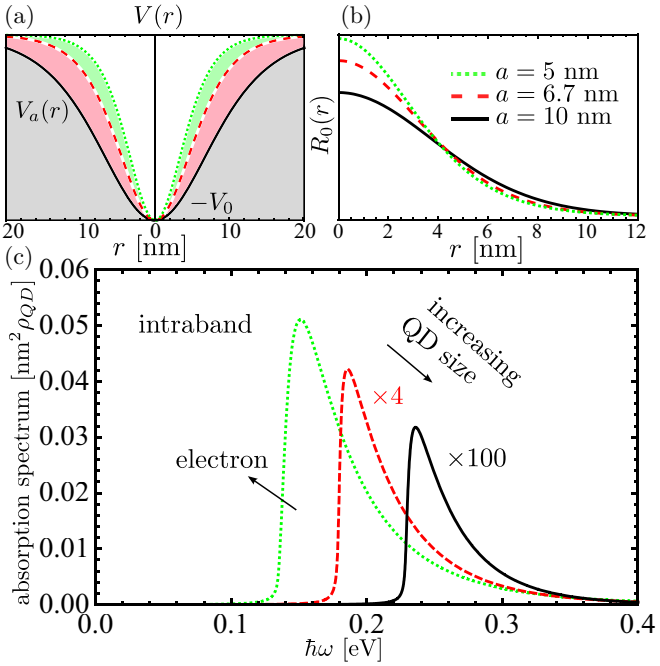

FIG. 2. (Color online) (a) Model confinement potentials for the QD system for different spatial extensions $a = 5$ nm, $a = 6.7$ nm, and $a = 10$ nm [cf. Eq. (17)]. (b) Electron QD ground state wave function for the model potentials in (a). (c) Intraband absorption spectra for epitaxially grown InAs QDs embedded in a GaAs bulk material, calculated beyond the plane wave approximation and with the QD ground state wave functions in (b). The pump pulse prepares a density in the ground state.

ergy eigenvalues due to the finite bulk volume. Using the parabolic dispersion Eq. (12), the corresponding approximate k values are calculated. Using the numerically correct bound QD ground state and unbound bulk wave functions, the intraband absorption spectra are calculated beyond the plane wave approximation. The result is depicted in Fig. 2(c) for different spatial extensions a. The absorption strength for the QD-continuum transitions are weak in comparison to interband transitions. However, it is has been shown that bound-continuum intraband absorption in InAs/GaAs QDs can indeed be measured by photoinduced absorption spectroscopy in Ref. [41] and using two-color photoexcitation spectroscopy in Ref. [42]. Each absorption starts at the energy [cf. the Heaviside function in Eq. (13)] sufficient to provide a transition between the bound QD state and the energetically closest continuum bulk state. Over frequency the spectrum reaches a maximum and then decreases since the Fourier transformation of the $\phi_{\lambda,0}(k)$ in k space also decreases [cf. Eq. (11)].

Figure 2 shows that the variation of QD parameters, i.e., the spatial extension of the QD confinement potential determined by a [cf. Eq. (17) and Fig. 2(a)], modifies the QD ground state wave function, shown in Fig. 2(b), and shows a strongly different shape in the spectra shown in Fig. 2(c). Since the presented spectra in Fig. 2(c) are numerically exact, these spectra are used to check whether Eq. (13) can be used to determine the spatial shape of the QD ground state wave function $\phi_{\lambda,0}(\mathbf{r})$ by using some independently measured spectrum α^0_λ. A Fourier transform of the extracted electron ground state wave function calculated with Eq. (13) from α^0_c generates the corresponding wave functions $R_0(r)$ in the spatial domain, (see Fig. 3 for a comparison with the original wave function).

The behavior of the reconstructed wave function with increasing spatial extension a is very similar to the original QD ground state wave function [cf. Figs. 3(a) and 3(b)]. In comparison to the original, the reconstructed wave functions are shifted by a constant to higher r values, shown in the inset of Fig. 3(a). Apart from that, the electron QD ground state wave functions can be extracted with good quality from the spectra. To show the power of our approach to obtain the QD extension and wave function, the localization length of the reconstructed bound wave function r^0_{rec} is determined and compared to the original r^0_{orig} [cf. the inset to Fig. 3(b)]. The linear fit has a gradient of one and an offset of 1.1 nm. The spatial extension of the wave function can only be determined within the error range, however, the reconstructed QD ground state wave function can be used to clarify QD spatial extensions relative to each other in all-optical measurements.

In conclusion, we presented a formula [Eq. (16)] to extract information about the spatial shape of QD electron ground

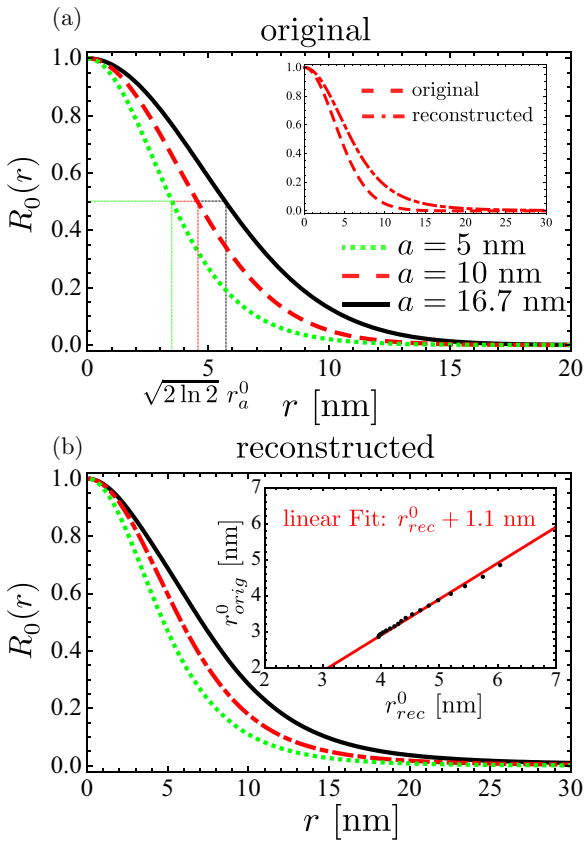

FIG. 3. (Color online) Comparison of (a) the original and (b) the reconstructed QD electron ground state wave function for different spatial extensions a. The reconstructed QD electron ground state wave functions are extracted from spectra beyond the plane wave approximation. The inset of (a) gives a direct comparison of the original and the reconstructed QD electron ground state wave function for $a = 10$ nm. The reconstructed one is shifted by a constant to higher r values. The FWHM gives the localization lengths r^0_{rec} and r^0_{orig}, which are plotted in the inset of (b) against each other. Apart from an offset of 1.1 nm, the QD wave functions can be extracted with good quality from the spectra.

state wave function from intraband absorption spectra. The proposed study is not limited to a specific QD system, and is generally applicable to other nanostructures embedded in a host providing continuum wave functions as final states for an absorption process.

We thank Nicolai Grosse and Oliver Esser for helpful discussions. Financial support by Deutsche Forschungsgemeinschaft (DFG) through Sonderforschungsbereich 787 is gratefully acknowledged. A.K. also acknowledges support via Bundesministerium für Bildung und Forschung within the Verbundprojekt "Nano-III-V-PINs".

[1] K. J. Vahala, Nature (London) **424**, 839 (2003).
[2] Q. Qiao, B. H. Li, C. Shan, J. S. Liu, J. Yu, X. H. Xie, Z. Z. Zhang, T. B. Ji, Y. Jia, and D. Z. Shen, Mater. Lett. **74**, 104 (2012).
[3] L. Brahim and M. Orrit, Rep. Prog. Phys. **68**, 1129 (2005).
[4] D. Bimberg, E. Stock, A. Lochmann, A. Schliwa, J. A. Tofflinger, W. Unrau, M. Munnix, S. Rodt, V. A. Haisler, A. I. Toropov, A. Bakarov, and A. K. Kalagin, IEEE Photonics J. **1**, 58 (2009).
[5] A. J. Nozik, Physica E **14**, 115 (2002).
[6] W. H. Jiang, H. Z. Xu, B. Xu, X. L. Ye, J. Wu, D. Ding, J. B. Liang, and Z. G. Wang, J. Cryst. Growth **212**, 356 (2000).
[7] R. L. Sellin, C. Ribbat, M. Grundmann, N. N. Ledentsov, and D. Bimberg, Appl. Phys. Lett. **78**, 1207 (2001).
[8] A. F. Tsatsul'nikov, A. R. Kovsh, A. E. Zhukov, Y. M. Shernyakov, Y. G. Musikhin, V. M. Ustinov, N. A. Bert, P. S. Kop'ev, Z. I. Alferov, A. M. Mintairov, J. L. Merz, N. N. Ledentsov, and D. Bimberg, J. Appl. Phys. **88**, 6272 (2000).
[9] N. N. Ledentsov, V. A. Shchukin, M. Grundmann, N. Kirstaedter, J. Böhrer, O. Schmidt, D. Bimberg, V. M. Ustinov, A. Y. Egorov, A. E. Zhukov, P. S. Kop'ev, S. V. Zaitsev, N. Y. Gordeev, Z. I. Alferov, A. I. Borovkov, A. O. Kosogov, S. S. Ruvimov, P. Werner, U. Gösele, and J. Heydenreich, Phys. Rev. B **54**, 8743 (1996).
[10] I. Robert-Philip, E. Moreau, S. Varoutsis, J. Bylander, M. Gallart, J. M. Gérard, and I. Abram, J. Lumin. **102-103**, 67 (2003).
[11] C. Robert, C. Cornet, P. Turban, T. Nguyen Thanh, M. O. Nestoklon, J. Even, J. M. Jancu, M. Perrin, H. Folliot, T. Rohel, S. Tricot, A. Balocchi, D. Lagarde, X. Marie, N. Bertru, O. Durand, and A. Le Corre, Phys. Rev. B **86**, 205316 (2012).
[12] D. B. Williams and C. B. Carter, *Transmission Electron Microscopy: A Textbook for Materials Science*, 2nd ed. (Springer, Berlin, 2009), Vol. 1.
[13] B. Fultz and J. M. Howe, *Transmission Electron Microscopy and Diffractometry of Materials*, 3rd ed. (Springer, Berlin, 2008).
[14] J. C. H. Spence, *High-Resolution Electron Microscopy*, 3rd ed. (Oxford University Press, Oxford, UK, 2009).
[15] R. J. Warburton, C. S. Dürr, K. Karrai, J. P. Kotthaus, G. Medeiros-Ribeiro, and P. M. Petroff, Phys. Rev. Lett. **79**, 5282 (1997).
[16] R. J. Warburton, C. Schulhauser, D. Haft, C. Schäflein, K. Karrai, J. M. Garcia, W. Schoenfeld, and P. M. Petroff, Phys. Rev. B **65**, 113303 (2002).
[17] J. J. Finley, M. Sabathil, P. Vogl, G. Abstreiter, R. Oulton, A. I. Tartakovskii, D. J. Mowbray, M. S. Skolnick, S. L. Liew, A. G. Cullis, and M. Hopkinson, Phys. Rev. B **70**, 201308 (2004).
[18] O. D. D. Couto, J. Puebla, E. A. Chekhovich, I. J. Luxmoore, C. J. Elliott, N. Babazadeh, M. S. Skolnick, A. I. Tartakovskii, and A. B. Krysa, Phys. Rev. B **84**, 125301 (2011).
[19] B. Eichenberg, S. Dobmann, H. Wunderlich, A. Seilmeier, L. E. Vorobjev, D. A. Firsov, V. Panevin, and A. A. Tonkikh, Physica E **43**, 1162 (2011).
[20] L. E. Vorobjev, D. A. Firsov, V. A. Shalygin, N. K. Fedosov, V. Yu Panevin, A. Andreev, V. M. Ustinov, G. E. Cirlin, V. A. Egorov, A. A. Tonkikh, F. Fossard, M. Tchernycheva, Kh. Moumanis, F. H. Julien, S. Hanna, A. Seilmeier, and H. Sigg, Semicond. Sci. Technol. **21**, 1341 (2006).
[21] A. Damascelli, Z. Hussain, and Z. X. Shen, Rev. Mod. Phys. **75**, 473 (2003).
[22] F. Quochi, M. Dinu, L. N. Pfeiffer, K. W. West, C. Kerbage, R. S. Windeler, and B. J. Eggleton, Phys. Rev. B **67**, 235323 (2003).
[23] G. Dasbach, T. Baars, M. Bayer, A. Larionov, and A. Forchel, Phys. Rev. B **62**, 13076 (2000).
[24] S. Dommers, V. V. Temnov, U. Woggon, J. Gomis, J. Martinez-Pastor, M. Laemmlin, and D. Bimberg, Appl. Phys. Lett. **90**, 033508 (2007).
[25] J. Gomis-Bresco, S. Dommers, V. V. Temnov, U. Woggon, M. Laemmlin, D. Bimberg, E. Malić, M. Richter, E. Schöll, and A. Knorr, Phys. Rev. Lett. **101**, 256803 (2008).
[26] D. S. Chuu, C. M. Hsiao, and W. N. Mei, Phys. Rev. B **46**, 3898 (1992).
[27] I. Affleck and P. Simon, Phys. Rev. Lett. **86**, 2854 (2001).
[28] H. J. Krenner, M. Sabathil, E. C. Clark, A. Kress, D. Schuh, M. Bichler, G. Abstreiter, and J. J. Finley, Phys. Rev. Lett. **94**, 057402 (2005).
[29] N. Liu, B. S. Prall, and V. I. Klimov, J. Am. Chem. Soc. **128**, 15362 (2006).
[30] H. Haug and S. Koch, *Quantum Theory of the Optical and Electronic Properties of Semiconductors*, 5th ed. (World Scientific, Singapore, 2009).
[31] E. Pazy, Semicond. Sci. Technol. **17**, 1172 (2002).
[32] Band structure of the valence band: $\epsilon_{v,k} = -\frac{\hbar^2 k^2}{2m_h} - \Delta E_v^0 + \epsilon_{v,0}$.
[33] P. Boucaud, S. Sauvage, and J. Houel, C. R. Phys. **9**, 840 (2008).
[34] B. P. Fingerhut, M. Richter, J.-W. Luo, A. Zunger, and S. Mukamel, Phys. Rev. B **86**, 235303 (2012).
[35] The potential height for the conduction band is assumed to be $V_0^c = 0.35$ eV.
[36] Comsol Multiphysics 4.3b, www.comsol.com.
[37] A. J. Williamson, L. W. Wang, and A. Zunger, Phys. Rev. B **62**, 12963 (2000).
[38] The effective mass in units of m_0^* is $m_e^* = 0.065$, $m_{hh}^* = 0.5$, and $m_{lh}^* = 0.076$.
[39] E. A. Muljarov and R. Zimmermann, Phys. Rev. Lett. **93**, 237401 (2004).
[40] B. T. Miller, W. Hansen, S. Manus, R. J. Luyken, A. Lorke, J. P. Kotthaus, S. Huant, G. Medeiros-Ribeiro, and P. M. Petroff, Phys. Rev. B **56**, 6764 (1997).
[41] S. Sauvage, P. Boucaud, J. M. Gérard, and V. Thierry-Mieg, Phys. Rev. B **58**, 10562 (1998).
[42] Y. Harada, T. Maeda, and T. Kita, J. Appl. Phys. **113**, 223511 (2013).